

# Eroding Ribbon Thermocouples: Impulse Response and Transient Heat Flux Analysis

March 24, 2005

David R Buttsworth<sup>1</sup>

Faculty of Engineering and Surveying  
University of Southern Queensland  
Toowoomba, 4350  
Australia

Robert Stevens, & C Richard Stone  
Department of Engineering Science  
University of Oxford  
Parks Road, Oxford, OX1 3PJ  
England

---

<sup>1</sup>corresponding author

## Abstract

We have investigated a particular type of fast-response surface thermocouple to determine if it is appropriate to use a one dimensional transient heat conduction model to derive the transient surface heat flux from the measurements of surface temperature. With these sensors, low thermal inertia thermocouple junctions are formed near the surface by abrasive wear. Using laser excitation, we obtained the impulse response of these commercially available devices. The response of particular sensors can vary if new junctions are created by abrasive wear. Furthermore, the response of these sensors was found to deviate substantially from the one dimensional model and varied from sensor to sensor. The impulse response was simulated with greater fidelity using a two dimensional finite element model, but three dimensional effects also appear to be significant. The impact of these variations on the derived heat flux is assessed for the case of measurements in an internal combustion engine. When the measured impulse response is used to derive the surface heat flux, the apparent reversal of heat flux during the expansion stroke does not occur.

## 1 Introduction

Surface junction thermocouples have been used for many years in various applications including boiling studies [1], internal combustion engine heat flux measurements [2], aerothermodynamics experiments [3],[4], and ballistics research [5], [6]. The eroding ribbon element thermocouple is a type of commercially available surface junction thermocouple [7] which has been used in similar applications. For example, a number of boiling studies [8],[9],[10], and internal combustion engine heat transfer studies [11],[12],[13],[14], have used eroding ribbon thermocouples.

The construction of an eroding ribbon thermocouple is illustrated in Figs. 1 and 2. The thermocouple materials (type K in this case) are ribbon elements  $25\ \mu\text{m}$  thick and are insulated from each other using  $5\ \mu\text{m}$  thick mica sheets. The surface thermocouple junction can be created by either metallic plating [10], or by drawing an abrasive surface or a sharp implement across the thermocouple as this creates small metallic elements that bridge the insulation at the surface [11].

It is normally assumed that the transient heat conduction process within the sensor is one dimensional so that a relatively simple model can be applied to deduce the surface heat flux from the measured surface temperature history. Illustrative examples of such one dimensional models are described in Section 2. In an attempt to improve the validity of such one dimensional assumptions, the material surrounding the thermocouple is sometimes chosen to match that of the engine component into which the sensor is inserted [12] (an aluminium alloy in our case), or the thermocouple is insulated from the component using a small air gap [12] or an insulating material [2].

However, with the eroding thermocouple construction, there are at least four different materials which could induce multi-dimensional heat conduction effects and contribute to the response of the sensor to a given heat flux at the surface: the positive thermocouple material, the negative thermocouple material, the insulation (mica), and the surrounding material (an aluminium alloy in our case). Previous users of these sensors have not demonstrated that the one dimensional assumption is justified over the relevant range of time scales.

Sensor calibrations on relatively long time scales (from about 0.1 to 1 s) have been performed using a tungsten-halogen lamp to provide a step heat flux input to the sensor [15],[13]. Results indicate that the sensitivity of the sensor (the rise in surface temperature) is somewhat higher than would be estimated using thermal properties of the surrounding material alone. Thus it appears likely that there is a contribution from the insulating material (mica) or the thermocouple materials that persists to these times.

Calibrations on shorter time scales have been performed by Kovačs and Mesler [16] and Buttsworth [17] for surface junction thermocouples of a coaxial construction. The insulation between the thermocouple materials was found to affect the response on millisecond times scales using a flash tube discharge technique [16] and on microsecond time scales using a shock tube calibration technique [17]. An influence from the different thermocouple materials was also identified on millisecond time scales using impacting water droplet calibrations [17].

Finite element modelling of fast response thermocouples [18],[19] has demonstrated the likely existence of multi-dimensional heat conduction. In the eroding thermocouple simulations of [19] it was demonstrated that on the microseconds time scales, the response of the sensor was dominated by the thermocouple material and the insulation. On the milliseconds time scales, heat was conducted away from the thermocouple junctions and the insulation by the surrounding aluminium alloy. However, even at 10 ms the temperature response of the sensor still remained more than 40% higher than it would have been if the substrate was actually a homogeneous aluminium alloy and semi-infinite one dimensional conduction prevailed.

To experimentally identify the actual response of eroding ribbon thermocouples, we have used a pulse of laser energy to induce a thermal response in these sensors. Gatowski et al. [15] used a laser to check the response time of an eroding thermocouple, but the results were not interpreted to yield other information on the step or impulse response characteristics. In contrast with other studies on the response of eroding ribbon and other surface junction thermocouples, we have been able to interpret our response measurements and use them to derive the surface heat flux from measurements of the surface temperature in a practical configuration of interest, an internal combustion engine.

## 2 Deduction of Heat Flux using a One Dimensional Model

Conventional approaches to the deduction of the surface heat flux from the measured surface temperature history assume the unsteady heat conduction is in a direction perpendicular to the surface of the sensor. With the further assumption of constant thermal properties within the sensor, the governing unsteady heat conduction equation is,

$$\frac{\partial \theta}{\partial t} = \alpha \frac{\partial^2 \theta}{\partial x^2}, \quad (1)$$

where  $t$  is time,  $x$  is distance from the surface of the sensor,  $\alpha$  is the thermal diffusivity of the sensor material, and  $\theta$  is the temperature within the sensor relative to the time averaged value at the same location,

$$\theta(x, t) = T(x, t) - \bar{T}(x). \quad (2)$$

For internal combustion engine applications, the common approach is to obtain a series solution to Eq. (1) from which the unsteady component of the surface heat flux history can be expressed as a series in terms of the engine speed, sensor thermal properties, and Fourier coefficients. The Fourier coefficients are identified from the Fourier series representation of the ensemble averaged temperature history [20],[21]. The steady component of the surface heat flux can be estimated using Fourier's Law and the sensor thermal conductivity if the temperature is also measured at a known depth from the sensor surface.

However, when cycle-to-cycle variations are of interest or when steady periodic conditions do not prevail, a transient solution to Eq. (1) is more appropriate. Considering the boundary conditions,

$$-k \frac{\partial \theta}{\partial x} = q \quad \text{at} \quad x = 0 \quad (3)$$

and

$$\theta = 0 \quad \text{at} \quad x = \infty, \quad (4)$$

the solution of Eq. (1) can be written [22],

$$\mathcal{L}\{q\} = \sqrt{\rho c k} \sqrt{s} \mathcal{L}\{\theta_s\}, \quad (5)$$

where  $q$  is the unsteady component of the surface heat flux,  $\theta_s$  is the unsteady component of the surface temperature,  $\rho$ ,  $c$ , and  $k$  are the density, specific heat, and conductivity respectively,  $\mathcal{L}$  denotes the Laplace transformation, and  $s$  is the Laplace variable. Taking the inverse Laplace transformation of Eq. (5) gives,

$$q = \frac{\sqrt{\rho ck}}{\sqrt{\pi}} \int_0^t \frac{d\theta}{d\tau} \frac{1}{\sqrt{t-\tau}} d\tau. \quad (6)$$

When implemented as a suitable discrete approximation, Eq. (6) allows deduction of the unsteady surface heat flux from the surface temperature history if conditions of one dimensional unsteady heat conduction prevail.

### 3 Step and Impulse Responses

We have investigated the applicability of the one dimensional heat conduction model to eroding ribbon thermocouples. Because we have done this using what is essentially an impulse of energy (see Section 4), it is now appropriate to consider some step and impulse response relationships.

For a step in surface heat flux at  $t = 0$ ,  $\mathcal{L}\{q\} = q_{\text{step}}/s$ , and Eq. (5) can be rearranged to give,

$$\mathcal{L}\{\theta_{s,\text{step}}\} = \frac{q_{\text{step}}}{\sqrt{\rho ck}} \frac{1}{s^{3/2}}, \quad (7)$$

which has the inverse Laplace transformation,

$$\theta_{s,\text{step}} = \frac{2q_{\text{step}}}{\sqrt{\pi}\sqrt{\rho ck}} \sqrt{t}. \quad (8)$$

The more general solution for the temperature change at any point in the semi-infinite substrate for one dimensional heat conduction can be found in heat transfer texts (eg [23]),

$$\theta_{\text{step}}(x, t) = \frac{2q_{\text{step}}\sqrt{t}}{\sqrt{\pi}\sqrt{\rho ck}} \exp\left(\frac{-x^2}{4\alpha t}\right) - \frac{q_{\text{step}}x}{\sqrt{\alpha}\sqrt{\rho ck}} \operatorname{erfc}\left(\frac{x}{2\sqrt{\alpha t}}\right). \quad (9)$$

For an impulse in energy applied to the surface at  $t = 0$ ,  $\mathcal{L}\{q\} = e_{\text{impulse}}$ , and the surface temperature becomes

$$\mathcal{L}\{\theta_{s,\text{impulse}}\} = \frac{e_{\text{impulse}}}{\sqrt{\rho ck}} \frac{1}{\sqrt{s}}, \quad (10)$$

which has the inverse Laplace transformation

$$\theta_{s,\text{impulse}} = \frac{e_{\text{impulse}}}{\sqrt{\pi}\sqrt{\rho ck}} \frac{1}{\sqrt{t}}. \quad (11)$$

Provided the thermal properties of the substrate are constant, the sensor can be regarded as a linear time invariant system and thus the unit impulse response is the derivative of the unit step response,

$$\theta_{s,\text{unit impulse}} = \frac{d\theta_{s,\text{unit step}}}{dt}, \quad (12)$$

and this is easily confirmed for the case of a semi-infinite one dimensional substrate by considering Eq. (8) and Eq. (11) with  $q_{\text{step}} = 1 \text{ W/m}^2$  and  $e_{\text{impulse}} = 1 \text{ J/m}^2$ .

Equation (12) applies not only for the case of semi-infinite one dimensional heat conduction, but also for multi-dimensional heat conduction problems with multi-material substrates (provided the thermal properties of all substrate materials are constant).

For the case of  $\sqrt{\rho ck} = 20 \times 10^{-3} \text{ J/m}^2\text{Ks}^{1/2}$  and  $\alpha = 50 \times 10^{-6} \text{ m}^2/\text{s}$ , the unit impulse response derived from Eq. (9) is presented in Fig. 3 for a number of different substrate depths. The semi-infinite impulse response at the surface of the substrate is a straight line with a slope of  $-1/2$  on the logarithmic axes of Fig. 3 because it varies with  $t^{-1/2}$  (Eq. 11).

## 4 Apparatus for Impulse Response Experiments

The impulse response of 5 different sensors was identified by sequentially positioning each sensor in the centre of a pulsed laser beam. The general arrangement is illustrated in Fig. 4. The beam was provided by a Continuum Powerlite 8010 Q-switched Nd:Yag (1064 nm in the fundamental) laser system frequency doubled (to 532 nm) at a repetition rate of 10 Hz. The beam had a diameter of approximately 10 mm and was very uniform in intensity – no structure was observed within the beam both when examining single-shot burn marks (photosensitised paper, Laser SOS) or when using a high-power visualiser (Solar TII) in the fundamental. Three different beam energies were used during the experiments. The beam energies reported in Table 1 were measured using a digital power meter (Scientech model 435) and a volume-absorbing thermopile with single-shot resolution.

The temperature of the reference thermocouples (see Fig. 1) was monitored using a hand-held thermocouple meter (Digitron). In each sensor, the reference junction was sufficiently deep that changes in reference junction temperature were not registered at this location during the experiments. The surface junction (see Fig. 2) was wired with the reference junction such that it produced a differential output relative to the reference thermocouple. This differential output signal was amplified using a multi-channel amplifier based on the Burr Brown INA110 chip configured with a gain of 500. For internal combustion engine experiments (see Section 7), the amplifier outputs are normally filtered using a 13 kHz low-pass RC filter, but for the impulse response experiments, this filter was removed on one channel giving the amplifier a measured rise time (10-90 %) of  $3.6 \mu\text{s}$ .

The duration of the laser pulse was approximately 10 ns (measured using a photodiode) for the case of the 23 mJ pulses. The amplifier we have used restricts our investigation of the sensor response to times larger than a few microseconds and the manufacturer of the eroding ribbon element thermocouples claims inherent response times of a similar magnitude. Thus the time scale of the energy delivered by the laser is around three orders of magnitude smaller than the minimum thermocouple response time scales of practical interest. It is therefore reasonable to treat the configuration as an impulse response experiment and to analyse the surface temperature measurements on this basis.

Output from the thermocouple amplifier was recorded on a Tektronics TDS3052 500 MHz 10 GS/s digital storage oscilloscope and averaged over a total of 512 laser pulses. The actual sampling rate was either 1, 5, or 50 MS/s depending on the experiment, but a total of 10000 samples were recorded in every case.

Results from the impulse response experiments are summarised in Table 1. The third column of this table indicates the temperature rise measured by the surface junction at a time 0.1 ms after the pulse of laser energy.

## 5 Impulse Response Results

Figures 5, 6, 7, and 8 illustrate results from the impulse response experiments. Sensor impulse responses are generally presented from the peak value following the laser pulse (which generally occurred at a time between 2 and  $4 \mu\text{s}$ ) up to the maximum time for which the data was recorded. Logarithmic axes are convenient because of the rapid decay in the impulse response. The theoretical semi-infinite one dimensional impulse response is also presented on these figures as the broken lines.

The measurements and theoretical results in Figs. 5, 6, 7, and 8 have been offset vertically for the purpose of presentation. However, each experimental result has been labelled with the measured temperature change at 0.1 ms after the laser pulse and this allows cross referencing via Table 1.

Table 1: Summary of impulse response experiments

sensor label	pulse energy (mJ)	$T(t = 0.1 \text{ ms})$ ( $^{\circ}\text{C}$ )
I	270	19.1
I	23	3.71
I	—+	0.0625
12	270	23.1
12	23	3.50
12	23	2.76
II	270	28.9
II	23	3.60
1	270	22.1
1	23	5.21
7	270	4.38
7	23	0.588

+ not measured but probably  $< 1 \text{ mJ}$

For both sensors I and 12 (Fig. 5 and Fig. 6), results are presented for three different (re-made) surface thermocouple junctions. Typically an open circuit was created at the surface junction by operating the laser at a higher power to ablate the surface and/or by abrading the surface with 1200 grit paper and then cleaning the surface. New surface junctions were then created by drawing 320 grit paper across the surface in a direction perpendicular to the ribbon elements.

For sensor I it can be observed (Fig. 5) that each of the different surface junctions produce an impulse response that follows the semi-infinite one dimensional theory reasonably well for the period from 0.1 ms to 1 ms. Differences between the response of the different surface junctions of sensor I are apparent for times  $< 0.1 \text{ ms}$ . In contrast, for sensor 12 (Fig. 6), there are substantial differences in the slope of the response within the period from 0.1 ms to 1 ms for the different surface junctions.

Figure 7 presents results from sensors II and 1 and also includes an impulse response obtained using two dimensional finite element modelling [19]. In this model, the sensor was treated as planar and symmetrical about the centre plane of the middle mica sheet (see Fig. 2). Thus, the difference in the thermal properties of the two thermocouple materials were ignored. Representative values for  $\sqrt{\rho ck}$  and  $\alpha$  were adopted for the mica, the thermocouple material, and the aluminium alloy.

In contrast with sensor I, the decay of the impulse response of sensors II and 1 is noticeably more rapid than predicted by the one dimensional theory in the period from 0.1 ms to 1 ms. The two dimensional

finite element result appears to model the impulse response better than the one dimensional theory – the two dimensional model predicts an impulse response that decays more rapidly than the one dimensional theory.

The impulse response from the finite element model presented in Fig. 7 for times greater than 1ms has actually been extrapolated from the response at 1 ms using a power law matching the slope of the impulse response at this time. This was necessary because the finite element model was only 1 mm deep with an insulated boundary condition at this depth [19]. The thermal diffusivity in the aluminium alloy was assumed to be  $50 \times 10^{-6} \text{ m}^2/\text{s}$ , so the effects of the finite depth of the model would be registered at the surface soon after 1 ms.

The decay of the measured impulse responses becomes significantly faster than that of the two dimensional model for times greater than 2 ms. The sensors were arranged to give surface temperature measurements relative to their respective reference junction temperatures. Thus it is reasonable that the impulse response of our sensors will approach 0 after the heat has penetrated to the depth of the reference junction (consider the difference between the impulse responses in Fig. 3 at  $x = 0 \text{ mm}$  and say  $x = 4 \text{ mm}$ ). However, the semi-infinite one dimensional theory predicts that the impulse response of a differential surface temperature measurement with a reference junction at a depth of 4.76 mm in an aluminium alloy substrate ( $\sqrt{\rho ck} = 20 \times 10^{-3} \text{ J/m}^2\text{Ks}^{1/2}$  and  $\alpha = 50 \times 10^{-6} \text{ m}^2/\text{s}$ ) will remain within 1% of the absolute surface temperature impulse response until 24.5 ms – an order of magnitude larger than the times observed in our experiments.

The increased rate of decay of the impulse response for times greater than 2 ms is therefore likely to be a heat conduction effect in the third dimension that was not considered in the two dimensional model. Surface thermocouple junctions may be formed anywhere along the exposed length of the ribbon which almost extends to the stainless steel wall. Some junctions will be closer to the stainless steel than others and the observed response will be an average value over all of the junctions. The diameter of the aluminium alloy within the stainless steel wall is 3.76 mm. Assuming a uniform distribution of junctions across the surface of the ribbon elements, the average junction distance from the stainless steel will be less than 1.88 mm, the radius of the aluminium alloy. Estimating the thermal penetration distance as [22],

$$x \approx 4\sqrt{\alpha t}, \quad (13)$$

and taking  $\alpha = 50 \times 10^{-6} \text{ m}^2/\text{s}$ , we calculate a thermal penetration distance of 1.3 mm in 2 ms. Thus it is reasonable to postulate that it is a heat transfer effect associated with the stainless steel that is responsible for the decay in impulse response observed at around 2 ms.

The impulse response for sensor 7 (Fig. 8) is strikingly different from the other sensors. On visual inspection, the surface of sensor 7 appeared quite different to the other sensors and this suggests that it has had quite a different work history, or has sustained some damage relative to the other sensors that were tested. Based on the results in Fig. 8, it is likely that this sensor has a number of thermocouple junctions at varying depths. The result labelled “theory: distributed depth” in Fig. 8 was generated assuming the net sensor response is the summation of a surface junction response (with a weighting of 0.25) and the response from a junction at a depth of 0.4 mm (with a weighting of 0.75). With the addition of other junctions with different depths and weightings, it is possible to improve the simulation of the observed response, but the conclusion remains the same – the “surface” junction of this sensor is actually distributed over different depths.

## 6 Deduction of Heat Flux using Impulse Responses

In our previous finite element modelling [19], we applied a step heat flux input at the surface of the sensor and differentiated the surface temperature history to obtain the impulse response. Model surface temperature histories corresponding to different temporal variations in surface heat flux were generated through convolution of the impulse response and the model surface heat flux variations. We now have measurements of sensor impulse response and we want to obtain the surface heat flux from the measured surface temperature history using these measured impulse responses.

Oldfield [24] describes a number of efficient ways to perform the required deconvolution using impulse response filtering techniques when analytical models for substrate behaviour are available. With the Oldfield approach, an impulse response filter is designed using suitable analytical basis functions. We have adopted this approach except that our basis functions are a step in heat flux and the corresponding change in surface temperature which is obtained by either: 1) integrating the measured impulse response; 2) using the two dimensional finite difference model step response; or 3) using the one dimensional semi-infinite analytical solution. The three representative unit step responses (ie the changes in surface temperature for  $q_{\text{step}} = 1 \text{ W/m}^2$ ) are presented in Fig. 9.

The two dimensional finite element model response (Fig. 9) is as described in [19] except that a power law extrapolation is used from 1 ms onwards (see Section 5). The unit step response for sensor I presented in Fig. 9 was obtained by integrating the measured impulse response presented in Fig. 7 and scaling the result so that it matched the step response of the finite element model at 1 ms ( $3.45 \times 10^{-6} \text{ }^\circ\text{C}$ ). This was necessary because absolute calibrations could not be obtained from the laser impulse experiments due to the unknown absorptivities of the surfaces of the sensors. The semi-infinite one dimensional step response (Eq. 8) has likewise been scaled so that it matches the finite element model response at 1 ms

implying an effective value of  $\sqrt{\rho ck} = 10343 \text{ J/m}^2\text{Ks}^{1/2}$ .

## 7 Spark-Ignition Internal Combustion Engine Measurements

To illustrate how the actual impulse response of the sensor can affect the deduction of heat flux from measurements of transient surface temperature, we consider the application of these eroding sensors to the measurement of internal combustion engine heat flux.

Of particular interest is the reversal of heat flux during the expansion stroke which was first identified under motored conditions many years ago (eg [2]) but has apparently been observed under fired conditions more recently as well [14]. If the thermal boundary layer in the working gas was steady, heat would flow from the gas to the wall during the expansion stroke because of the elevated temperature of the working gas. However, a reversal of heat flow during the expansion stroke can be explained in the case of motored (and perhaps fired) operation on the grounds that the expansion occurs on a shorter time scale than that associated with the thermal diffusion in the boundary layer. This means the temperature gradient in the vicinity of the wall can reverse its direction with a sufficiently large and rapid drop in pressure.

In a previous publication [19], where the two dimensional finite element model of an eroding ribbon element thermocouple was introduced, it was suggested that at least part of the apparent reversal of heat flux observed in [14] could be attributed to the application of the simple one dimensional model for the transient conduction in the sensor substrate when a multi-dimensional model is necessary. Although we do not have impulse response measurements for the actual surface junctions that were used in the experiments of [14], we can nevertheless re-analyse the data using a representative impulse response measurement (sensor 1).

Details of the engine and the positions of the heat flux sensors are available in [14]. The engine was a single cylinder Rover K4 research engine operated at 1000rpm and part throttle with methane fuel at a relative air-fuel ratio,  $\lambda = 1.0$ . Cylinder pressure measurements averaged over 98 cycles for these conditions are presented in Fig. 10. Corresponding heat flux measurements are presented in Figs. 11 and 12.

To obtain the results in Figs. 11 and 12, the fluctuating component of the measured surface temperature was analysed using the impulse response filtering techniques described in Section 6 to give the heat flux for each of the 98 cycles. The results were then ensemble averaged to produce the results that are presented in Figs. 11 and 12. The time averaged temperature difference between the surface and reference junctions was approximately  $1^\circ\text{C}$  which amounts to a steady component of heat flux of around  $0.04 \text{ MW/m}^2$ .

When the measured surface temperature is treated with the one dimensional theory, the heat flux registers a significant reversal relative to the level at bottom dead centre, and this was observed in a previous publication [14]. The apparent reversal of heat flux is most obvious in the case of sensor 12, Fig. 12. When the measured temperature signals are processed using the response from the two dimensional finite element model, the reversal of heat flux does not occur in the case of sensor 2, and the magnitude of the reversal is reduced in the case of sensor 12. But when the surface temperature is treated with an experimentally-derived sensor response, the apparent reversal of heat flux is completely eliminated in both cases.

## 8 Conclusion

Care is required when using the eroding ribbon thermocouples that we have considered.

For the time scales less than 0.1 ms, different thermocouple junctions created on the same sensor can produce very different responses. For time scales between 0.1 ms and 1 ms, different junctions can still influence the sensor response, but the response is typically more consistent than for time scales less than 0.1 ms. The sensors do not generally follow a one dimensional response over any time scale. The sensor response can be simulated more accurately using a two dimensional model that accounts for transverse conduction effects, but such a model still does not adequately simulate the rapid decay in impulse response which is always observed from approximately 2 ms onwards. It appears likely that this rapid decay is associated with lateral conduction arising due to the presence of the stainless steel housing around the aluminium alloy substrate.

The use of either one dimensional or two dimensional models for the sensor response will lead to substantial errors in the inferred heat flux results. If a measured impulse response is available for a particular sensor or better still, for a particular junction, then it should be used to derive the heat flux from the surface temperature measurements.

### Acknowledgement

We wish to acknowledge the provision of an EPSRC Visiting Fellowship for DRB, the generous assistance of Dave Oude Nijeweme in the interpretation of the IC engine data, and Martin Oldfield for making available his Matlab scripts [24].

## References

- [1] F. D. Moore and R. B. Mesler, “The measurement of rapid surface temperature fluctuations during nucleate boiling of water”, *AIChE Journal*, vol. 7, pp. 620–624, 1961.
- [2] B. Lawton, “Effect of compression and expansion on instantaneous heat transfer in reciprocating internal combustion engines”, *Proc. Instn Mech. Engrs, Part A, Journal of Power and Energy*, vol. 201, pp. 175–186, 1987.
- [3] S. L. Gai and W. S. Joe, “Laminar heat transfer to blunt cones in high-enthalpy flows”, *J. Thermophysics Heat Transfer*, vol. 6, pp. 433–438, 1992.
- [4] C. Jessen, M. Vetter, and H. Gronig, “Experimental studies in the Aachen hypersonic shock tunnel”, *Z. Flugwiss. Weltraumforsch.*, vol. 17, pp. 73–81, 1993.
- [5] D. Bendersky, “A special thermocouple for measuring transient temperatures”, *Mech. Eng.*, vol. 75, pp. 117–121, 1953.
- [6] B. Lawton and G. Klingenberg, *Transient Temperature in Engineering and Science*, Oxford University Press, Oxford, 1996.
- [7] *Nanmac: Temperature Measurement Handbook Vol. VIII*, 9-11 Mayhew Street Framingham, MA 01701, USA. <http://www.nanmac.com/>.
- [8] M. Pasandideh-Fard, S. D. Aziz, S. Chandra, and J. Mostaghimi, “Cooling effectiveness of a water drop impinging on a hot surface”, *Int. J. of Heat and Fluid Flow*, vol. 22, pp. 201–210, 2001.
- [9] Y. M. Qiao and S. Chandra, “Boiling of droplets on a hot surface in low gravity”, *Int. J. of Heat Mass Transfer*, vol. 39, no. 7, pp. 1379–1393, 1996.
- [10] J. C. Chen and K. K. Hsu, “Heat transfer during liquid contact on superheated surfaces”, *J. Heat Transfer Trans ASME*, vol. 117, pp. 693–697, 1995.
- [11] A. C. Alkidas, “Heat transfer characteristics of a spark-ignition engine”, *J. Heat Transfer Trans ASME*, vol. 102, pp. 189–193, 1980.
- [12] A. C. Alkida and J. P. Myers, “Transient heat flux measurements in the combustion chamber of a spark-ignition engine”, *J. Heat Transfer Trans ASME*, vol. 104, pp. 62–67, 1982.
- [13] A. C. Alkidas, P. V. Puzinauskas, and R. C. Peterson, “Combustion and heat transfer studies in a spark-ignited multivalve optical engine”, *SAE Trans J. Engines*, vol. 99, pp. 817–830, 1990.
- [14] D. J. Oude Nijeweme, J. B. W. Kok, C. R. Stone, and L. Wyszynski, “Unsteady in-cylinder heat transfer in a spark ignition engine: experiments and modelling”, *Proc. Instn Mech. Engrs, Part D, Journal of Automobile Engineering*, vol. 215, pp. 747–760, 2001.

- [15] J. A. Gatowski, M. K. Smith, and A. C. Alkidas, “An experimental investigation of surface thermometry and heat flux”, *Exp. Therm. Fluid Sci.*, vol. 2, pp. 280–292, 1989.
- [16] Á. Kovács and R. B. Mesler, “Making and testing small surface thermocouples for fast response”, *Rev. Scientific Instr.*, vol. 35, pp. 485–488, 1964.
- [17] D R Buttsworth, “Assessment of effective thermal product of surface junction thermocouples on millisecond and microsecond time scales”, *Experimental Thermal and Fluid Science*, vol. 25, no. 6, pp. 409–420, 2001.
- [18] N S Jackson and M H Sandford, “An experimental assessment of instantaneous heat transfer within a highly rated DI truck engine”, in *Experimental Methods in Engine Research and Development*, Combustion Engines Group. IMechE, London, March 1988.
- [19] D R Buttsworth, “Transient response of an erodable heat flux gauge using finite element analysis”, *Proceedings of the Institution of Mechanical Engineers Part D (Journal of Automobile Engineering)*, vol. 216, pp. 701–706, 2002.
- [20] V. D. Overbye, J. E. Bennethum, O. A. Uyehara, and P. S. Myer, “Unsteady heat transfer in engines”, *SAE Transactions*, vol. 69, pp. 461–494, 1961.
- [21] G Borman and K Nishiwaki, “Internal-combustion engine heat transfer”, *Progress in Energy and Combustion Science*, vol. 13, pp. 1–46, 1987.
- [22] D. L. Schultz and T. V. Jones, “Heat-transfer measurements in short-duration hypersonic facilities”, AGARDograph 165, Advisory Group for Aerospace Research and Development, 1973.
- [23] F. P. Incropera and D. P. DeWitt, *Fundamentals of Heat and Mass Transfer*, John Wiley and Sons, New York, 5th edition, 2001.
- [24] M. L. G. Oldfield, “Guide to impulse response heat transfer signal processing”, OUEL Report 2233/2000, Department of Engineering Science, University of Oxford, 2000.

## List of Figures

1	General construction of the eroding thermocouples. . . . .	16
2	Detailed view of the surface junction of the eroding thermocouples. . . . .	16
3	Unit impulse response from the semi-infinite one dimensional theory with $\sqrt{\rho ck} = 20 \times 10^{-3} \text{ J/m}^2\text{Ks}^{1/2}$ and $\alpha = 50 \times 10^{-6} \text{ m}^2/\text{s}$ . . . . .	17
4	Arrangement for the eroding thermocouple impulse response experiments. . . . .	17
5	Results from the impulse response experiments – sensor I with 3 different junctions. . . .	18
6	Results from the impulse response experiments – sensor 12 with 3 different junctions. . . .	18
7	Results from the impulse response experiments – sensor II (two experiments with the same junction) and sensor 1 (one experiment). . . . .	19
8	Results from the impulse response experiments – sensor 7. . . . .	19
9	Unit step response for three cases. . . . .	20
10	Ensemble averaged cylinder pressure (98 cycles). . . . .	20
11	Ensemble averaged fluctuating heat flux (98 cycles) from sensor 2 (cylinder liner). . . . .	21
12	Ensemble averaged fluctuating heat flux (98 cycles) from sensor 12 (cylinder head). . . . .	21

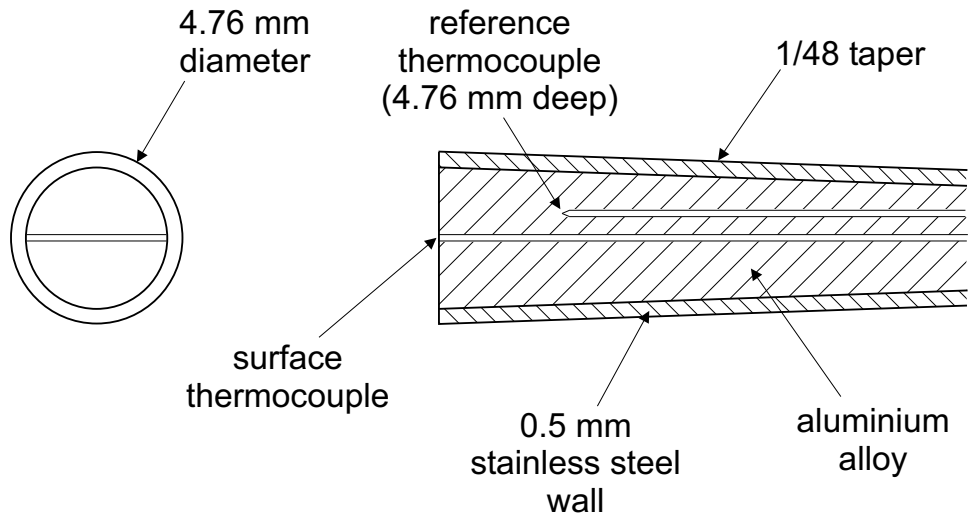


Figure 1: General construction of the eroding thermocouples.

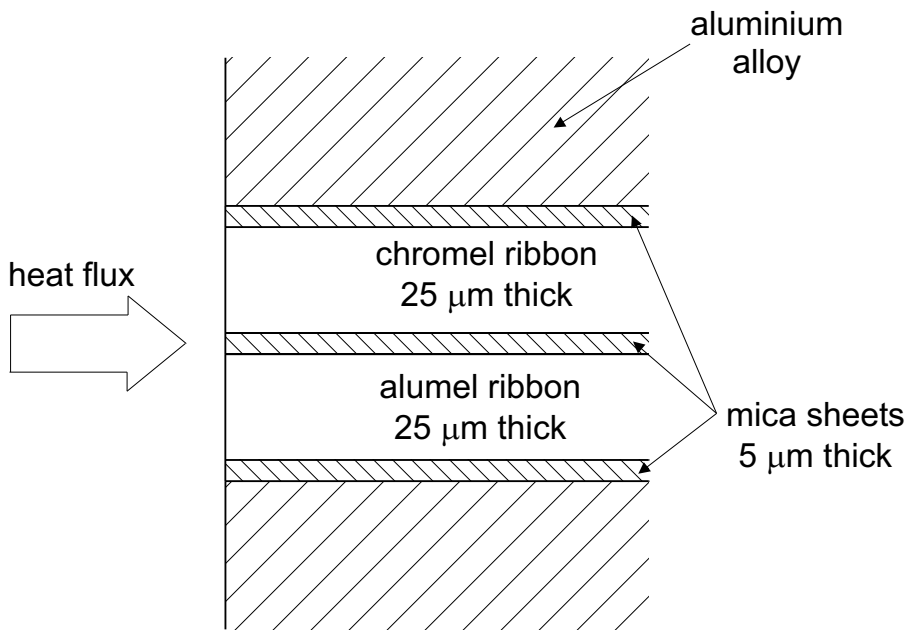


Figure 2: Detailed view of the surface junction of the eroding thermocouples.

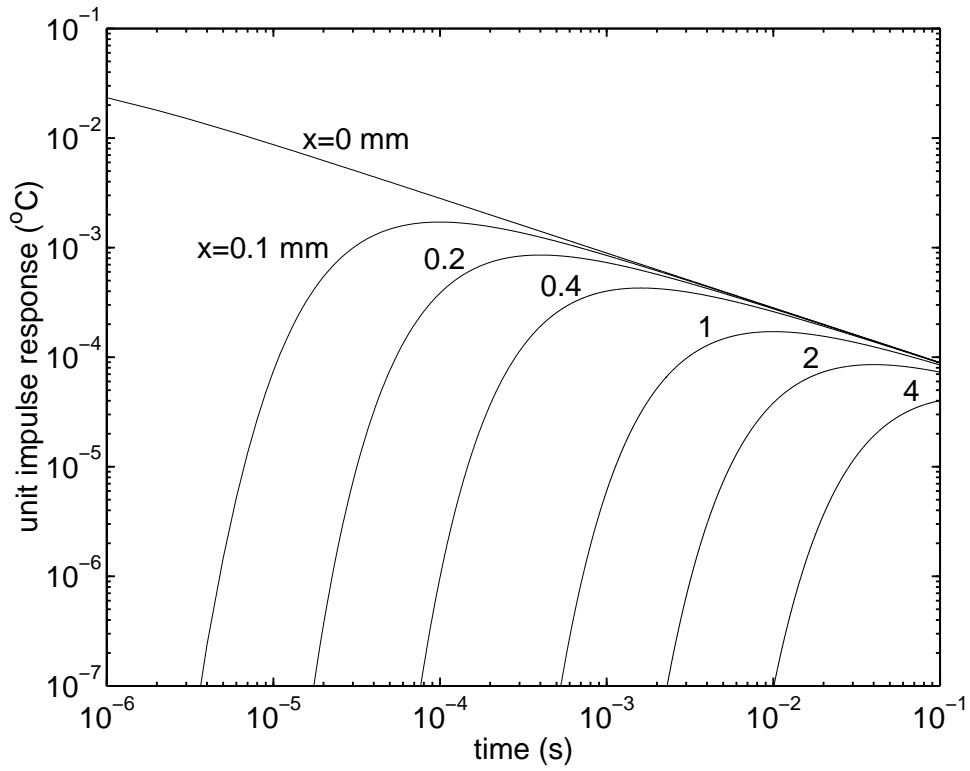


Figure 3: Unit impulse response from the semi-infinite one dimensional theory with  $\sqrt{\rho ck} = 20 \times 10^{-3} \text{ J/m}^2\text{Ks}^{1/2}$  and  $\alpha = 50 \times 10^{-6} \text{ m}^2/\text{s}$ .

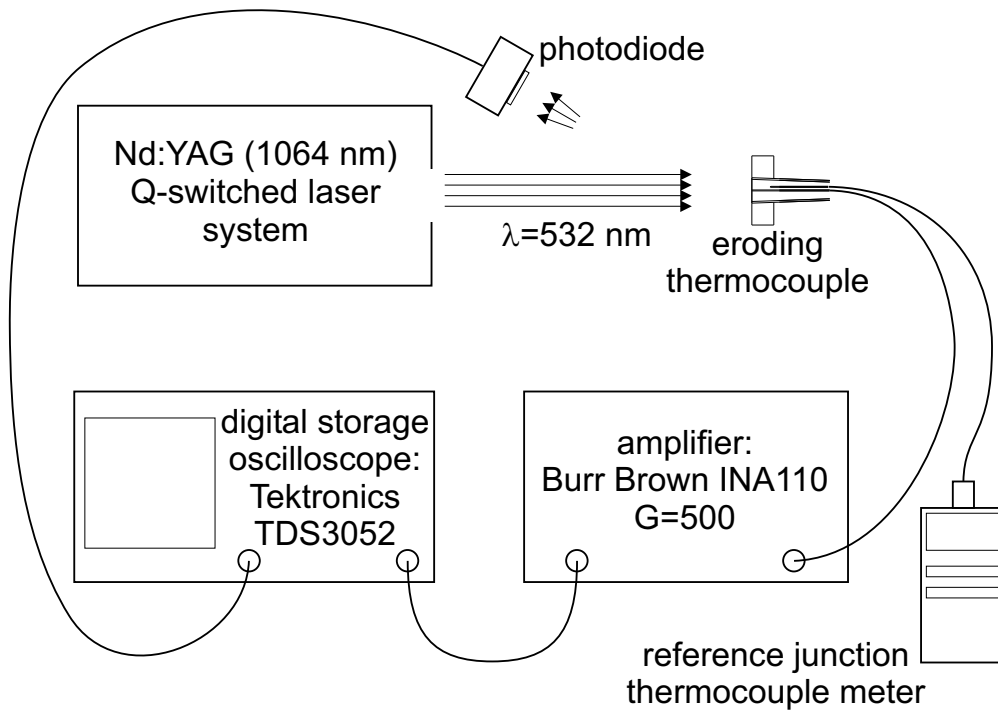


Figure 4: Arrangement for the eroding thermocouple impulse response experiments.

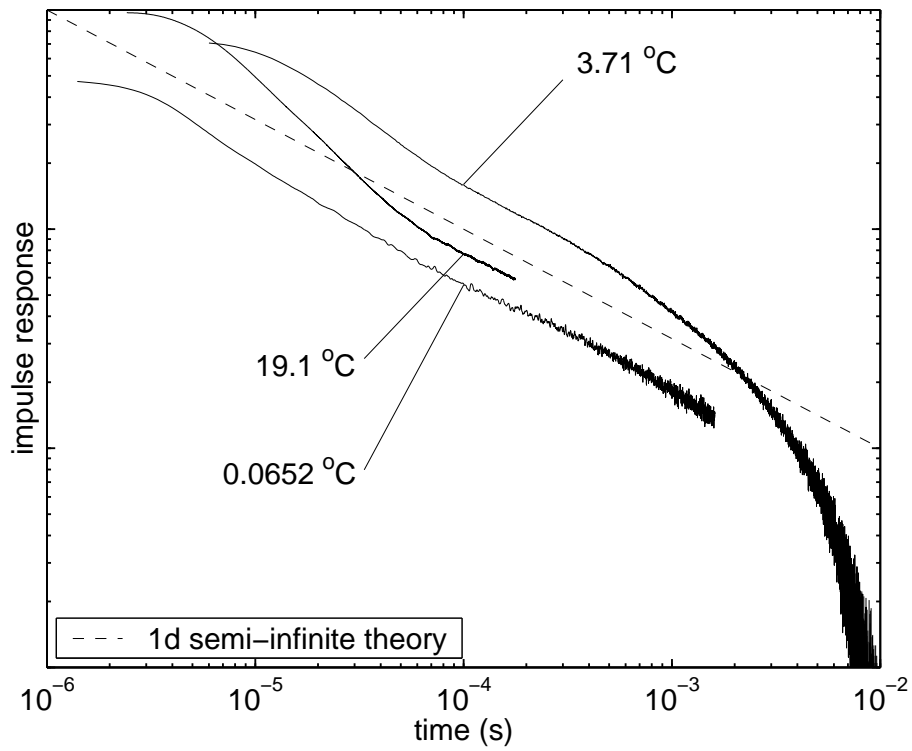


Figure 5: Results from the impulse response experiments – sensor I with 3 different junctions.

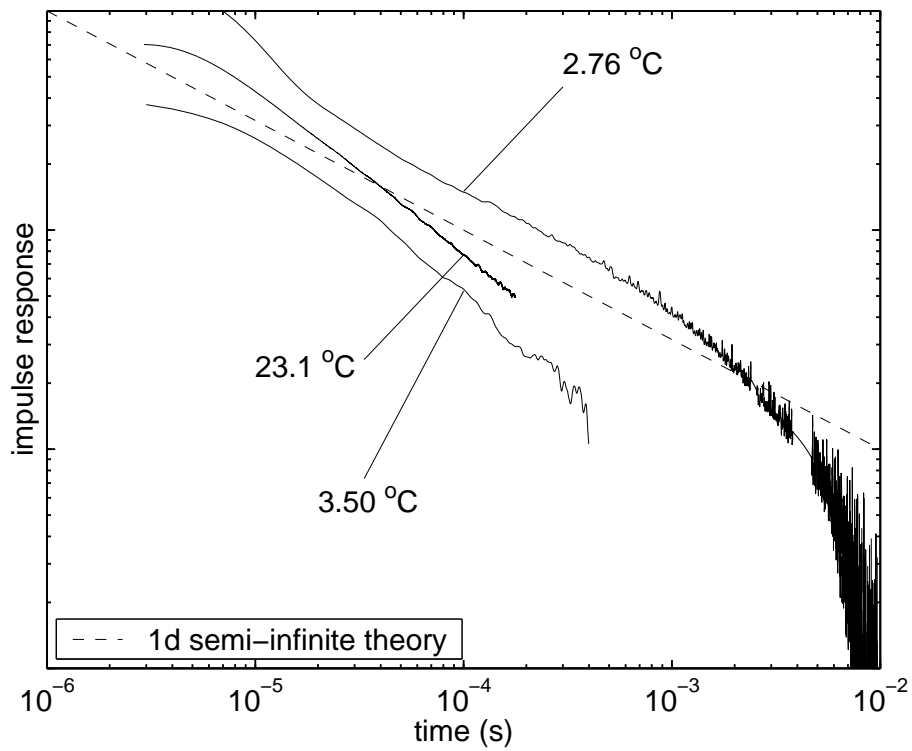


Figure 6: Results from the impulse response experiments – sensor 12 with 3 different junctions.

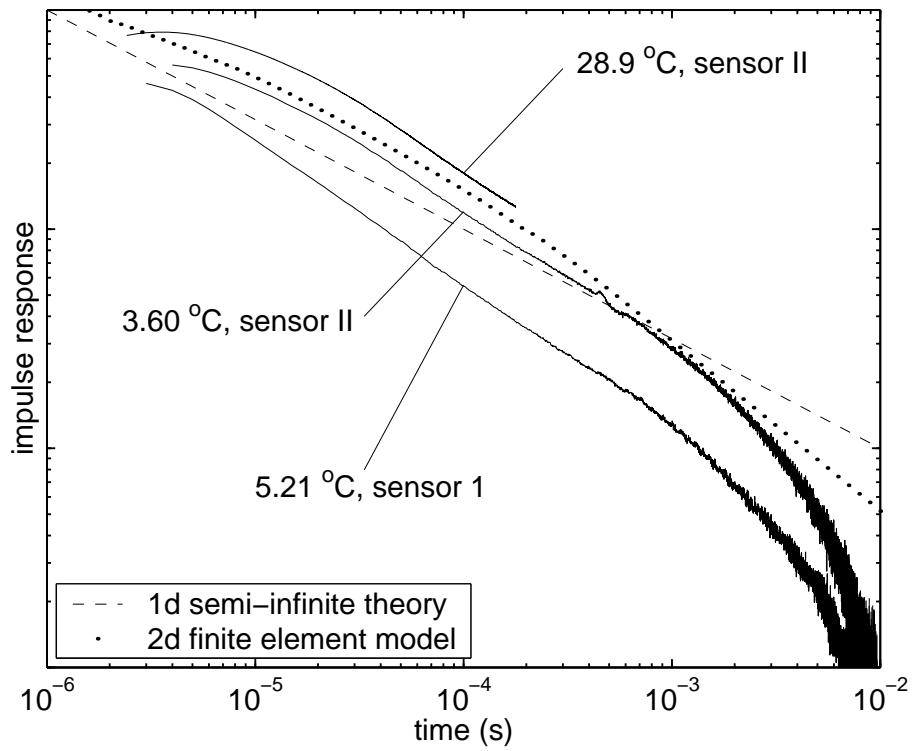


Figure 7: Results from the impulse response experiments – sensor II (two experiments with the same junction) and sensor 1 (one experiment).

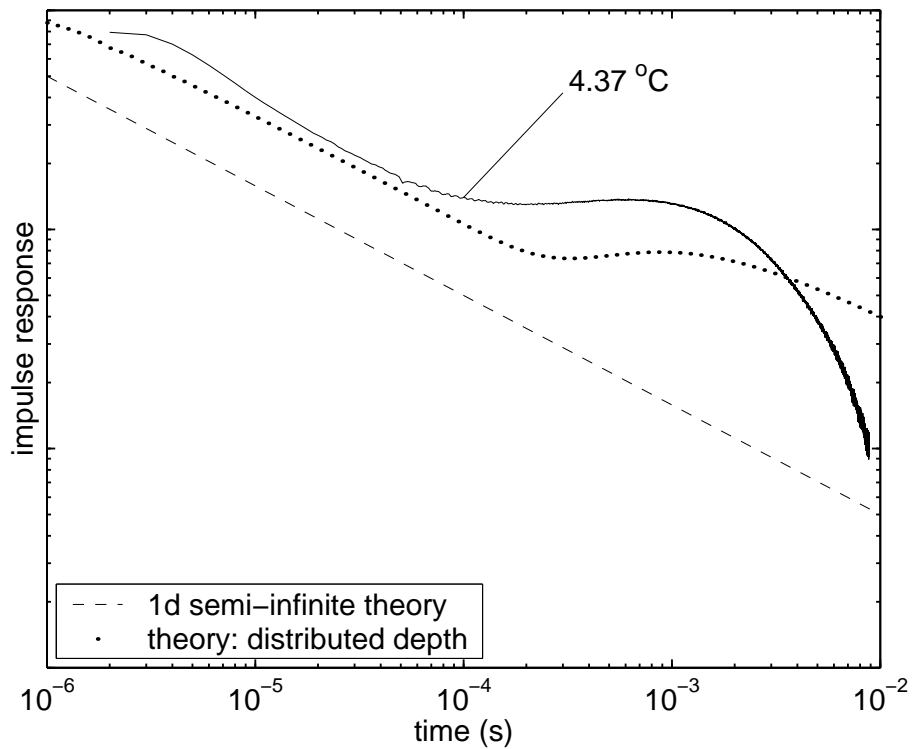


Figure 8: Results from the impulse response experiments – sensor 7.

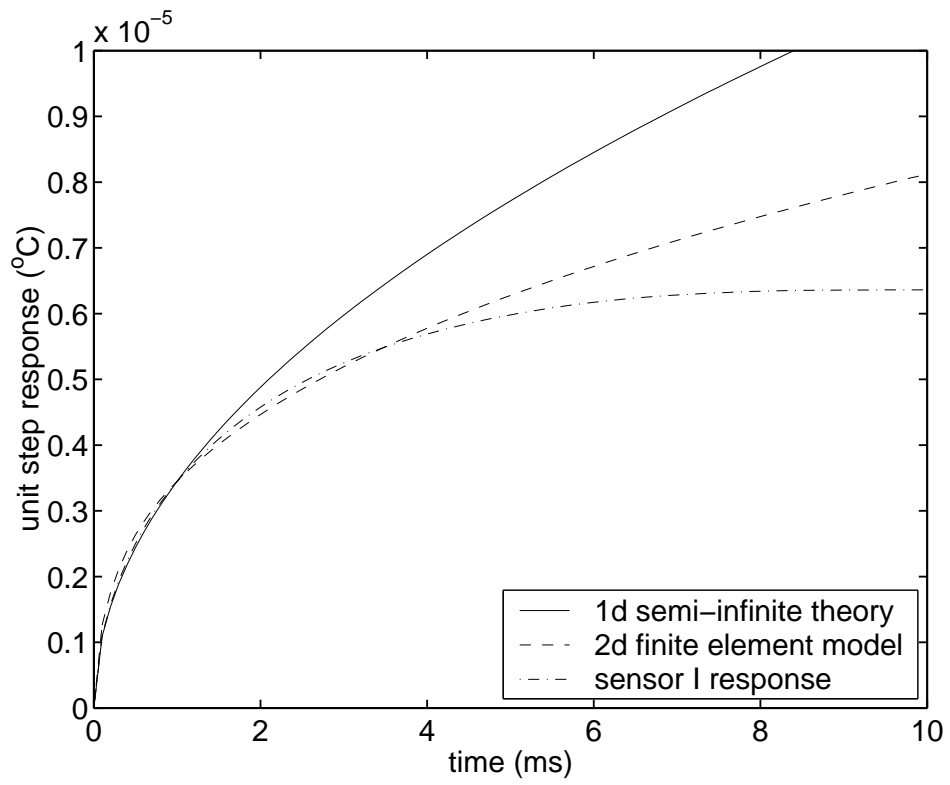


Figure 9: Unit step response for three cases.

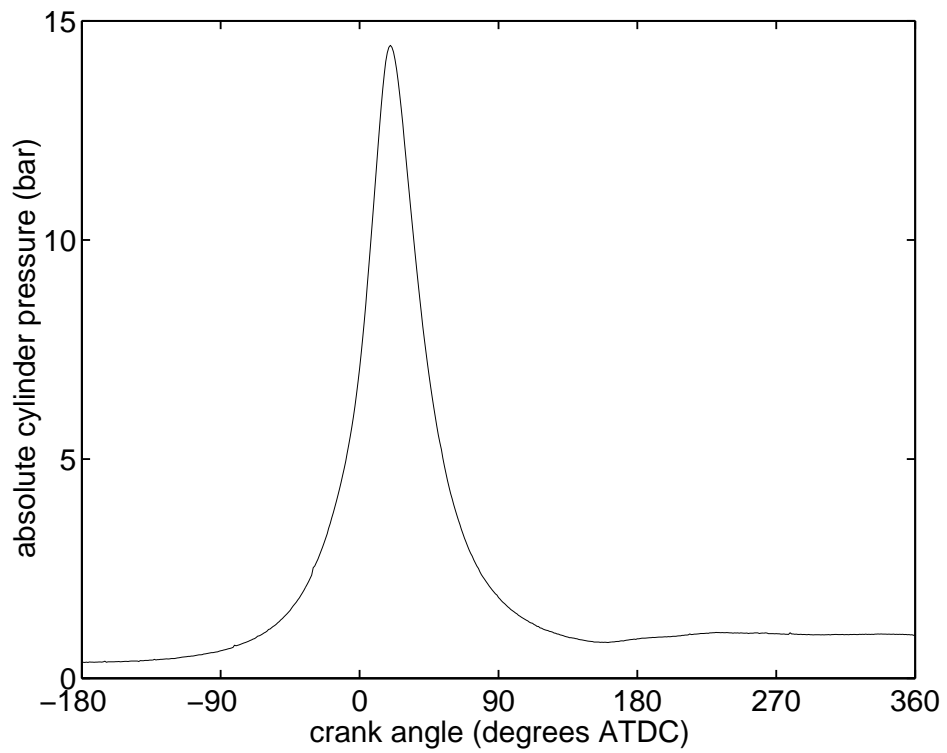


Figure 10: Ensemble averaged cylinder pressure (98 cycles).

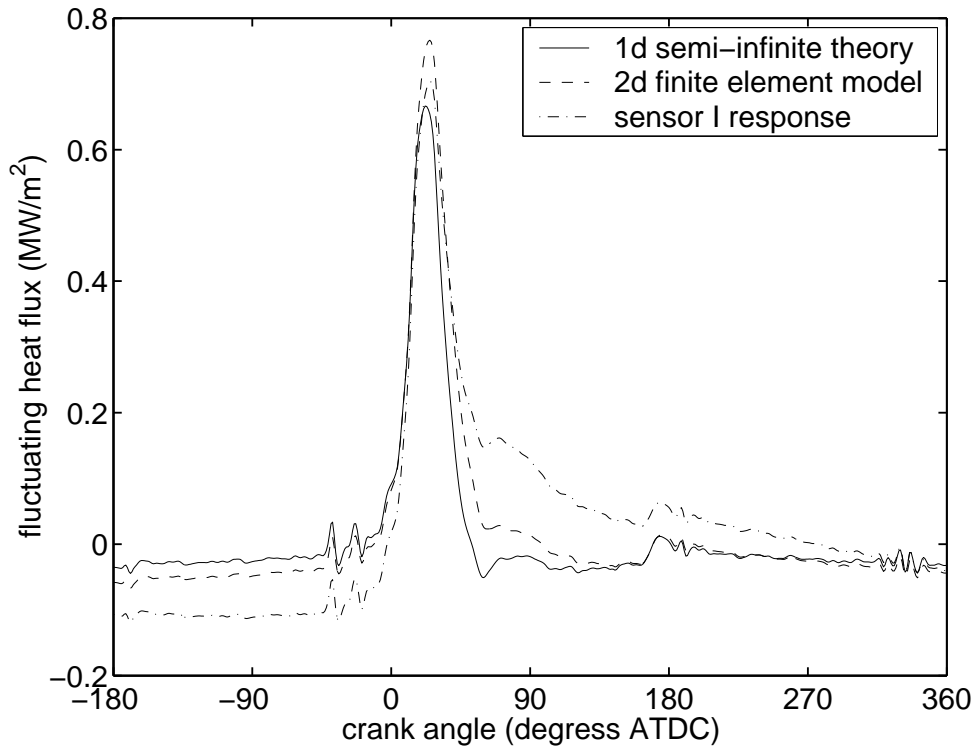


Figure 11: Ensemble averaged fluctuating heat flux (98 cycles) from sensor 2 (cylinder liner).

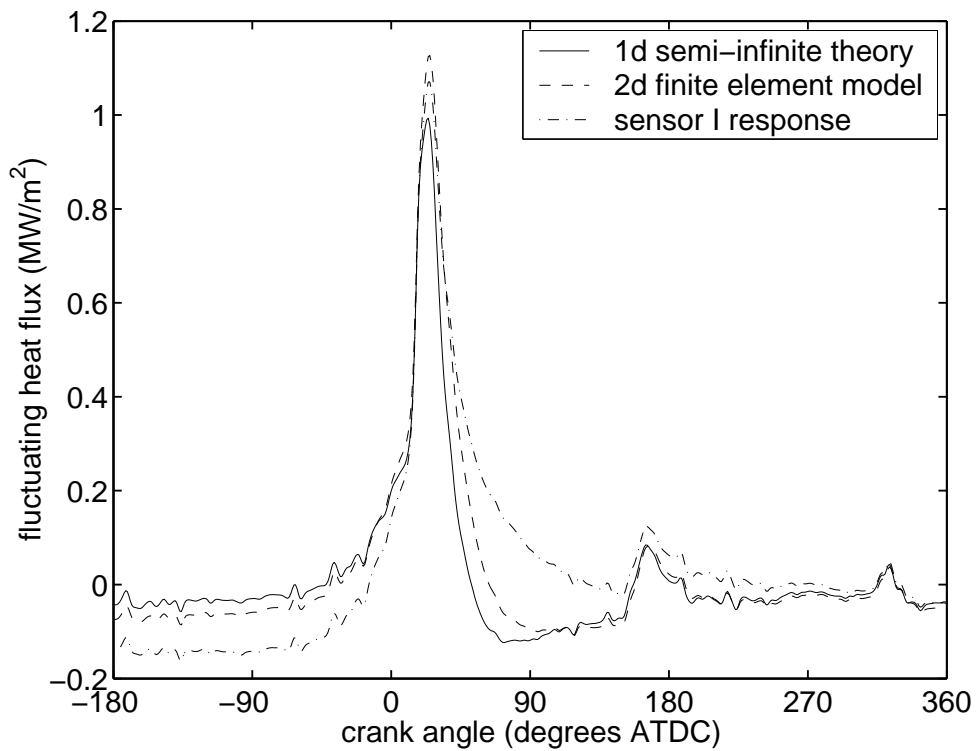


Figure 12: Ensemble averaged fluctuating heat flux (98 cycles) from sensor 12 (cylinder head).